Brodogradnja/Shipbuilding/Open access Volume 74 Number 2, 2023

Ahmet Yurtseven
Kaan Aktay

http://dx.doi.org/10.21278/brod74205

ISSN 0007-215X
eISSN 1845-5859

The numerical investigation of spindle torque for a controllable pitch propeller in feathering maneuver

UDC 629.5.035.55:629.5.017.3
Original scientific paper

Summary

Present paper studies the variation of the blade spindle torque in a controllable pitch propeller (CPP) during the feathering maneuver, which is one of the rare but most challenging propeller maneuvers in CPP operation. The knowledge of the spindle torque under different operating conditions is one of the key features for the CPP controller unit design. The aim of this study is determining the forces needed to be governed to control the blade motion of a CPP converted from a fixed pitch propeller and the scale effect on these forces. So as to obtain a realistic numerical setup, the time-dependent superposed motion of the main rotation of the propeller and the rotation of each blade around its axis is modeled using a hybrid overset/sliding mesh technique. The spindle torque values were calculated during the dynamical variation of the blade pitch in feathering maneuver, and a novel expression is recommended to non-dimensionalize the predicted spindle torque. The result revealed that the required torque values to rotate each blade during the propeller maneuver is rising up to a critical pitch angle. Further increment of the pitch angle results in lower spindle torque values. Furthermore, this critical pitch angle is inversely proportional to the propeller loading.

Key words: *Controllable pitch propeller; CPP; CFD; spindle torque; overset*

1. Introduction

There are different propulsion systems for commercial and military vessels. In general, the propulsion systems mounted to the stern are commonly preferred. The propellers are evaluated by the thrust produced, the amount of torque needed and the efficiency of the propeller depending on these parameters. Similarly, the most common parameters applied to define the propeller behaviors are propeller rotation, propeller diameter and vessel velocity. In recent years, the effects of the parameters on the propeller have been investigated due to high-speed and maneuvering capability needs [1-4].

Since the propeller revolution is linked to the main propulsion system driving the propeller, the flexible behaviors might be limited here. The idea to replace the propeller pitch to improve the propeller performance by keeping the main engine rotation the same appeared with controllable pitch propellers (CPP) [5]. CPP propellers first appeared in aviation applications based on the need to change the pitch of fixed pitch propellers during flight. In earlier times, propellers with different blade and hub materials were manufactured, the pitch determined for the flight conditions and the pitch was changed on the ground. However, it

was seen that the speed changes during the flight decreased the efficiency since the pitch is determined to maximize the efficiency based on the aircraft speed and propeller rotation. In order to improve this state, the aim was to change the propeller pitch depending on the aircraft user's needs during driving [6].

Due to the operational flexibility they offer, CPP's provide several advantages for marine applications, especially for naval ships [7]. The main difference between CPP and fixed pitch propellers is that CPP can rotate around its spindle axis to create different pitches. Investigating the hydrodynamic behaviors of the CPPs is vital to reveal the data necessary for propeller design and operation. Nguyen et al. [8] attempted to reveal the CPP general hydrodynamic structure and the effects of pitch rates on the thrust.

The knowledge gap due to challenges of working on CPPs were generally eliminated with different pitch propeller performance values in the Wageningen B series fixed pitch propeller (FPP) database. Despite few experimental studies, the studies on CPPs often focused on computational fluid dynamics (CFD). Ozturk et al. [9] used the Wageningen B series propeller database to systematically investigate the effect of propeller pitch on self-propulsion points in the vessels.

Few examples are encountered for experimental studies on CPP propellers. In studies that extensively published data on experimental studies on CPP propellers, a limited amount of spindle torque values were presented [10, 11].

Like the many other studies concerning the propeller design stage, CFD stands as a powerful tool to investigate the factors affecting the CPP design. Funeno et al. [12] both experimentally and numerically investigated the CPP pitch and propeller performance in commercial vessels with a large range. The authors identified the differences between the numerical results and experimental results for low advance coefficients and points near the neutral pitch. The authors recommended further studies, especially for neutral pitch points for the flow around the propeller. Rhee and Joshi [13] verified the DTMB P5168 model CPP test propeller experimental results by using CFD methods. Although the authors used CPP geometry, the rotation of the blades around their spindle axis was neglected. Kolakoti et al. [14] numerically investigated the propeller-body interaction for a CPP. Xiong et al. [15] investigated the propeller characteristics and the pressure distribution on the blades for open sea experimental conditions for blade geometries added to the CPP hub. It is possible to see applications for CPPs where the propeller is put inside a duct to increase the propeller efficiency. Bhattacharyya et al. [16] investigated the effects of different channel model scales on CPPs. Usta and Korkut [17] numerically investigated propeller cavitation characteristics for a CPP and twisted blade geometry. Zhou et al. [18] investigated the change of a CPP hydrodynamic performance by using different turbulence models. The authors obtained the closest results based on the experimental data with the RSM turbulence model and the closest values were with the k-$\boldsymbol{\varepsilon}$ model. The cavitation behaviors which are one of the most fundamental design parameters for propellers were also investigated in addition to the hydrodynamic performance. Arifin et al. [19] numerically investigated the cavitation behavior of CPP geometries with different pitch ratios, blade numbers and propeller diameters. Pourmostafa and Ghadimi [20] investigated the effects of a CPP hub diameter on the propeller characteristics with a proposed BEM solver. The authors revealed the propeller characteristic based on the non-dimensional hub diameter and propeller diameter.

One of the key parameters that limits the fundamental CPP design is the hydraulic driving units that give the angles to the blades and help them to sustain the given angles. These hydraulic units should be able to supply the pressure changes. The torque that rotates the blades and keeps them constant is the hydraulic piston-cylinder setup designed for the propeller hub and this is obtained with an oil distribution (OD) box that ensures correct

hydraulic oil distribution. This torque might correspond to different hydraulic pressures depending on the piston geometry. Altosole and Martelli [21] developed a mathematical motion model to assign and test oil behavior in a propeller hub for a CPP. The authors attempted to simulate the propeller operation. However, classic spindle torque data was used when the mathematical model was developed.

The connection between the blades and propeller hub for the CPP is called the wing bearing. Each blade can make a rotation movement around its own blade spindle passing through the blade hub center to create the propeller pitch. The torque that ensures this rotation movement is called the spindle torque. The propeller spindle torque is based on the thrust of the propeller and the propeller torque [22].

Since the behavior of the propeller hydraulic driving unit pressure is directly linked to the hydrodynamic effects on the blade, it is suitable to investigate the propeller spindle torque for the pressure change in the hydraulic driving unit. Martelli et al. [23] attempted to create a mathematical and numerical model for a CPP driving mechanism. The propeller spindle torque in the model was obtained by regression among the open water propeller test data which is called the semi-time-independent method. The authors determined that the hydraulic oil pressure in the propeller blade driving unit showed highly similar behavior to the blade spindle torque. This indicates that blade spindle torque can be used instead of the pressure behavior for studying hydraulic oil pressure.

There are only a few studies on propeller spindle torque in the literature. Just like all other propellers, it is expected that the impact of the cavitation in CPPs on the propeller design should be investigated. Jessup et al. [24] experimentally studied the propeller blade torque and investigated how the cavitation impacted the load on CPP blades. Tarbiat et al. [25] investigated the hydrodynamic behaviors of a CPP by using a certain number of pitches in an open-source CFD program by using the RANS methods. The authors attempted to answer the friction problem in the blade bearing [26]. The authors showed that the friction problem occurred when the spindle torque was higher than the friction torque. Liu et al. [27] investigated the hydrodynamic performance of a CPP under cavitation and non-cavitation conditions. The authors showed that the propeller blade spindle torque was a parameter linked to propeller pitch and advance coefficient. Pourmostafa and Ghadimi [28] investigated the time-dependent transition between the pitches. The authors investigated the effect of the pitch-changing speed of the blades on the track region behind the propeller. The authors didn't investigate the viscous effects due to the model used in the study. The authors showed that the pitch change created an instant peak value in the propeller thrust and the same effect was seen in the track region behind the propeller. The authors didn't investigate the blade spindle torque change during pitch change.

CPPs are designed to change the pitch angle to match the different vessel speeds and cruising conditions. However, these propellers can engage in rare maneuvers for feathering to cut out the propeller in conditions such as sudden speed decrease and sternway maneuver to go in the opposite direction, failure of a propulsion group (propeller or propulsion system) in a multi-propeller vessel. These maneuvers must be faster than the pitch change maneuvers at normal cruising speed. Therefore, the hydraulic driving units might need more capacity than under normal operating conditions.

The data for these rare maneuvering conditions for CPPs are highly limited in the literature. Additionally, most of the studies consider the propeller blade motion around its own axis time independently (changing the pitch angle on the primary geometry and analyzing the each angle independently) and the interaction between the propeller's main rotation movement and the rotation of the blades around their own spindle axis is neglected. Through the author's knowledge, it's the first time study for the numerical modeling of time-dependent, superposed CPP motion with the RANS approach.

The aim of this study is to parametrically investigate the blade spindle torque values (thus the force needed in hydraulic driving units) in different operating conditions of the propeller. The superposed transient-rotational motion of the propeller during the maneuver from full ahead pitch position to feathering position (feathering maneuver), which is one of the rare but most challenging maneuvers for CPP, was modeled via hybrid overset/sliding mesh approach. To examine the spindle torque results in a CPP, a novel non-dimensionalization method was proposed for the sake of better representation of the trends in the torque variation. Finally, pressure balance along the propeller blades were analyzed to understand the changes in the spindle torque under different operating conditions.

2. Numerical modelling

2.1. Governing equations

This study employed computational fluid dynamics (CFD) to solve the equations in the computer environment. The flow field was considered as three-dimensional, viscous, time-dependent and incompressible.

The governing equations, the continuity and Reynolds-Averaged Navier Stokes (RANS) equations are:

$$\frac{\partial U_i}{\partial x_i} = 0 \tag{1}$$

$$\rho\left(\frac{\partial U_i}{\partial t} + U_j \frac{\partial U_i}{\partial x_i}\right) = -\frac{\partial P}{\partial x_i} + \frac{\partial \tau}{\partial x_j} - \frac{\partial\left(\overline{\rho u_i' u_j'}\right)}{\partial x_j} \tag{2}$$

here U_i is the average velocity vector, u' is the turbulence velocity vector, $\left(\overline{\rho u_i' u_j'}\right)$ is the turbulence stress tensor, P is the average pressure, ρ is the density and μ is the dynamic viscosity.

$$\tau = \tau_{ij} = \mu\left(\frac{\partial U_i}{\partial x_j} + \frac{\partial U_j}{\partial x_i}\right) \tag{3}$$

here τ_{ij} is the average molecular stress tensor.

Additionally, a realizable k-$\boldsymbol{\varepsilon}$ turbulence model was preferred to model the turbulence field.

A commercial CFD tool, Simcenter Star CCM+ version 2020.3 was utilized in the study. The solver implements finite volume method to discretize the governing equations. Both spatial and temporal discretizations were done by second order accurate schemes to increase the accuracy. Well known SIMPLE algorithm was used for pressure-velocity coupling. Further information about the numerical solution can be found in the solvers manual [29].

2.2. Numerical approach

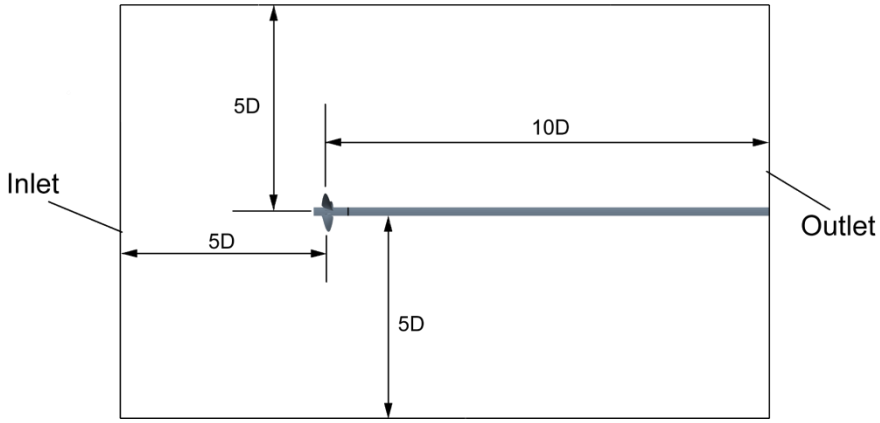

Fig. 1 Solution domain and the placing of the propeller

The solution domain given in Figure 1 was created for the computations flow around the propeller. The "D" letter in the figure represents the propeller diameter. The "Inlet" and "Outlet" boundary conditions in the solution domain were displaced depending on the rotation direction of the propellers.

The flow inlet surface boundary condition was set as uniform velocity inflow and the output surface boundary condition was set as "Pressure Outlet". The "Symmetry plane" boundary condition was used for the other surfaces. "No-slip conditions" were applied to the propeller blades and drive shaft surfaces.

This study was designed under open sea propeller test conditions and all analyses were conducted for this condition. The propeller blade maneuvers were used to change the blade angles to achieve propeller pitch. Accordingly, this study selected the most challenging scenario which is the transition from full ahead to feathering pitch position as shown in Figure 2.

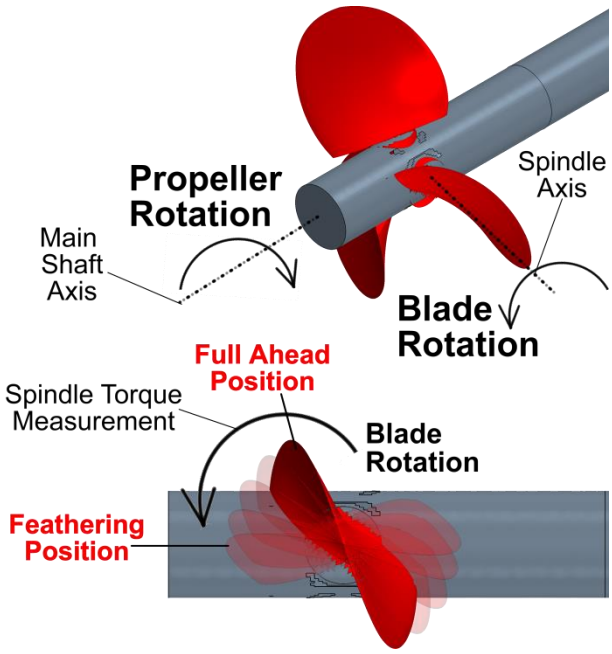

Fig. 2 Pitch maneuver investigated in the study

CPPs require additional motion model design compared to FPPs since the blades rotate around their own axis. The main rotation of the propeller around the drive spindle axis was modeled with "Rigid-Body Motion" which separates the volume from the solution with a cross-sectional surface. The rotation of the propeller blades around their axis was modeled

with an “Overset mesh” motion method. For propeller blade maneuver, these two motion models were super positioned in a hybrid form.

Throughout the study, the time step was selected to match the Courant-Friedrich-Lewy (CFL) number CFL < 1 condition, which corresponds to the maximum 6 degrees of propeller rotation.

2.3. Grid structure

Unstructured hexahedral elements were used to construct the solution domain, as seen in Figure 3. Several volumetric refinement regions were created around and in the slipstream of the propeller. Prismatic layer elements were used over the propeller surface, to accurately predict the high velocity gradients in the boundary layer.

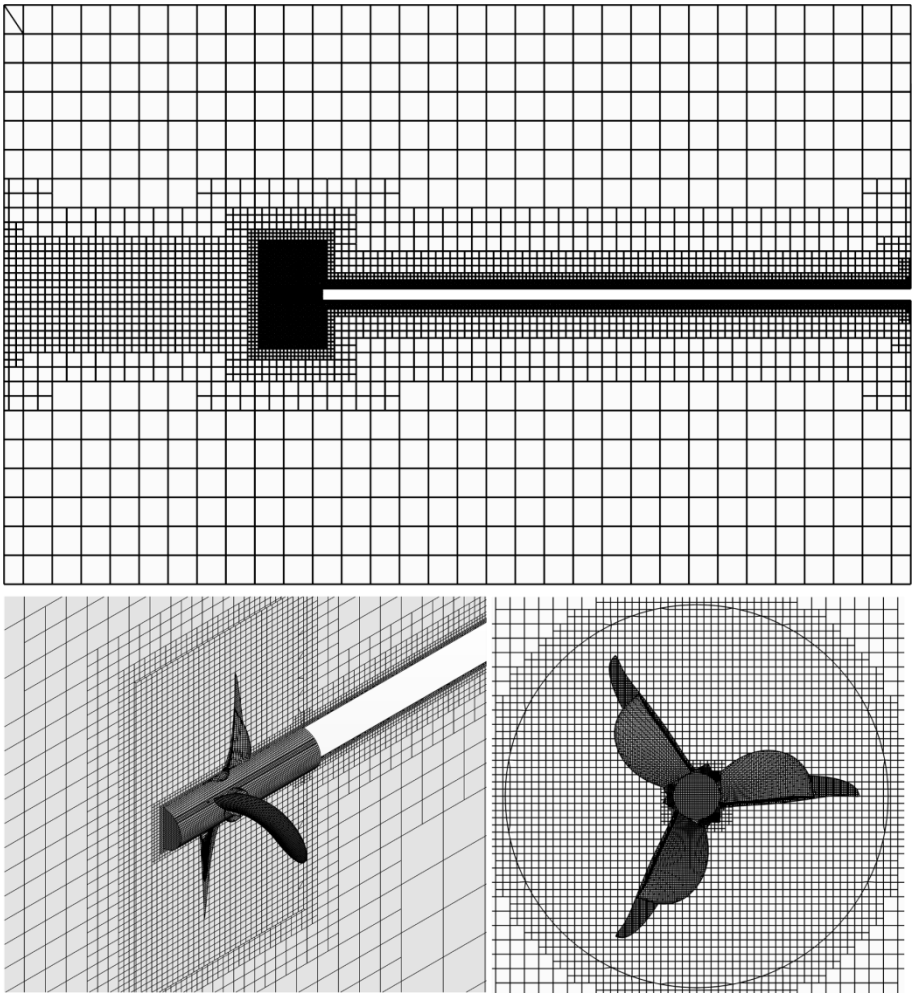

Fig. 3 The mesh structure and the refinement regions

The first node point near the wall was placed as to provide wall y^+ ($y^+ = u^*y/\nu$ where u^* is the reference velocity, y is the normal distance from the centroid to the wall in wall-adjacent cells and ν is the kinematic viscosity.) between 50 and 120. Figure 4 shows the Wall Y+ distribution on the CPP DTMB 4119 propeller blades for J = 0.5.

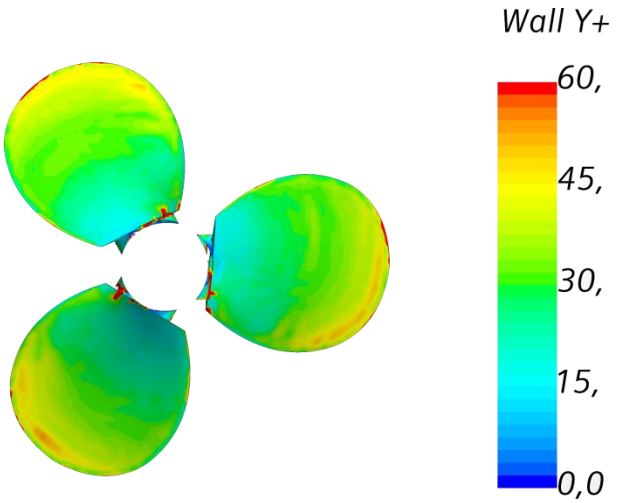

Fig. 4 CPP DTMB 4119 propeller Wall Y+ distribution for $J = 0.5$

The values used in the mesh dependency and time step dependency studies are given in Table 1.

Table 1 Mesh dependency and Time step dependency Values

	Cell Count	**Trust [N]**
Finer	3301742	642.72
Fine	1641564	641.67
Medium	809705	639.3
Coarse	404496	636.4
Coarser	200855	632.79

	Timestep	**Trust [N]**
Fine	0.0005	641.67
Medium	0.001	641.67
Coarse	0.002	637.91

3. Problem description

3.1. Propeller Geometry

In this study David Taylor Model Basin (DTMB) 4119 test propeller model was modified with a computer-aided design and an FPP was converted into a CPP. The main idea here is to take a propeller model that was originally designed to serve as a FPP and see whether it is possible to use it as a CPP or not. The FPP form of this propeller was included in numerous studies and this propeller was preferred as the test propeller for hydro-acoustic and cavitation fields in recent studies [30]. The propeller characteristics for the basis propeller are given in Table 2.

Table 2 DTMB 4119 Propeller Characteristics

D (m)	0.3048
Z	3
Blade Section	NACA66 a=0.8
Rotation direction	Right

The FPP DTMB 4119 propeller selected as the test propeller and the converted CPP DTMB 4119 propeller are depicted in Figure 5.

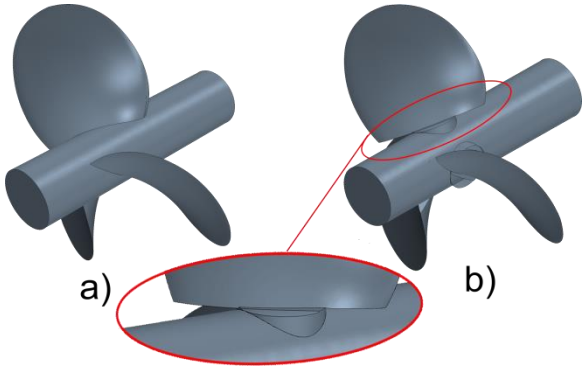

Fig. 5 a) FPP-DTMB 4119, b) CPP-DTMB 4119

There are small geometrical manipulations that were applied to the original DTMB 4119 propeller model to convert it to CPP. When Figure 5 is investigated, the FPP is cut from the stem part where the blades are connected to the main drive spindle and remounted to the main drive spindle to permit these blades to rotate around their own axis.

3.2. The Validation

Five different advance coefficients, J=0.500, J=0.700, J=0.833, J=0.900, and J=1.100, were tested to investigate the agreement of the numerical calculations with the experimental and numerical datas [31,32]. Figure 6 shows the comparison of the experimental data (EFD) and the numerical data (CFD).

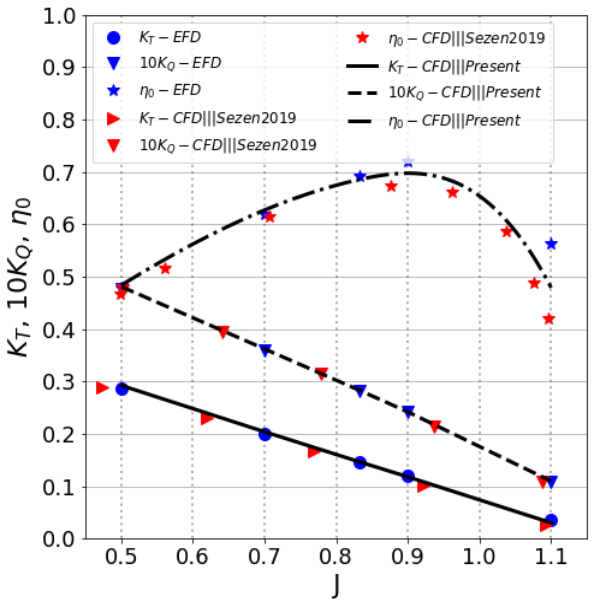

Fig. 6 Comparison of the numerical and the experimental data

The numerical and the experimental results show a fairly good agreement. After validating the numerical methodology with the DTMB 4119 propeller model, the CPP and FPP versions of the propeller were compared, to investigate possible performance variations arising from the conversion to CPP. The results of this comparison are given in Figure 7.

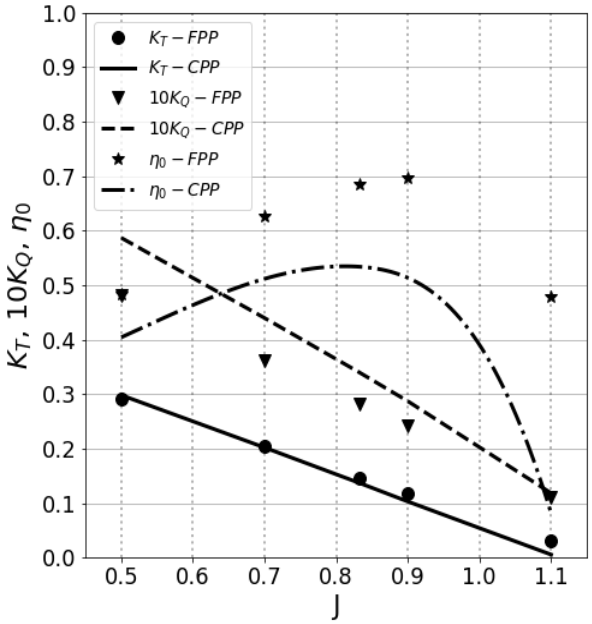

Fig. 7 The comparison of the FPP and the CPP versions of the propeller

It is seen that the thrust coefficient obtained from the CPP showed similar values to FPP. However, higher values for the torque coefficient were observed for lower advance coefficients while lower thrust coefficient values were obtained for higher advance coefficient. Therefore, the propeller efficiency was calculated at a low level. The lower thrust values were subjected to the geometrical adjustments at the blade near the hub connection.

4. Results

This section presents the CPP DTMB 4119 propeller hydrodynamic results for open sea propeller test conditions.

Non-dimensional coefficients to investigate the propeller performance are as advance coefficient (Eq. 4), thrust coefficient (Eq. 5), torque coefficient (Eq. 6) and propeller efficiency (Eq. 7):

$$J = \frac{V_a}{nD} \tag{4}$$

$$K_T = \frac{T}{\rho n^2 D^4} \tag{5}$$

$$K_Q = \frac{Q}{\rho n^2 D^5} \tag{6}$$

$$\eta_0 = \frac{K_T}{K_Q}\frac{J}{2\pi} \tag{7}$$

Additionally, the propeller rotation and blade spindle torque coefficient obtained from the rotation of the blades around their own spindle axis is shown in Eq. 8 [12].

$$K_{Q.b.lit} = \frac{Q_b}{\rho n^2 D^5} \tag{8}$$

Figure 8 compares the dimensional blade spindle torque values and coefficients non-dimensionalized with different approaches. However, when the trend of the dimensional torque values graph in Figure 8.a is examined, it is seen that the coefficient in the literature does not explain the results well. To increase the clarity and readability of the results, also

provide a better physical representation, modified blade spindle torque coefficients given in Eq. 9 were recommended.

$$K_{Q.b} = \frac{Q_b}{\rho n^2 D^5 J^2} \tag{9}$$

Here T (N) is the propulsion, Q (Nm), D (m) is the propeller diameter, n (rps) is the propeller rotation, ρ (kg/m3) is the density and V_a (m/s) is the average flow speed entering the solution volume. Additionally, Q_b (Nm) is the blade spindle torque. The data were reprocessed for the recommended blade spindle torque coefficient (Eq. 9) and shown in Figure 8.c. As seen from the figure, the data is close to the trend when the data in Figure 8.a and the similarity in physical behavior is clearer. This expression was employed as the blade spindle torque coefficient for the remaining sections of this study.

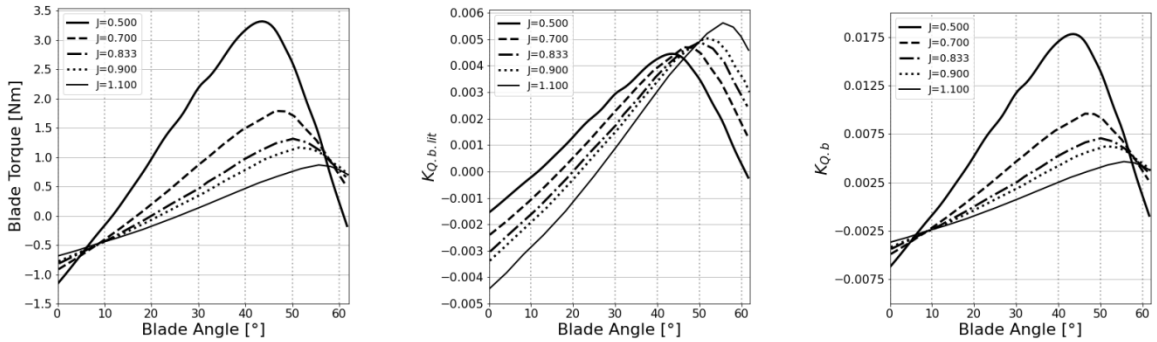

a) b) c)

Fig. 8 a) Dimensional blade spindle torque. b) Blade spindle torque coefficient calculated with Eq. 8 c) Blade spindle torque coefficient calculated with Eq. 9

It is seen that the propeller main shaft rotation rate is eliminated in the newly proposed dimensionless blade spindle torque coefficient. Blade spindle torque coefficient graphs obtained by doubling the propeller main shaft rotation rate and doubling the ship speed to keep the advance coefficient constant are shown in Figure 9.

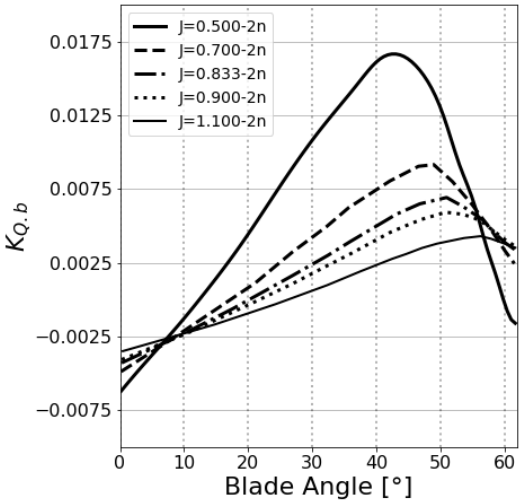

Fig. 9 Blade spindle torque coefficient calculated with Eq. 9 using doubling propeller main shaft rotation rate

The time-dependent solutions of the motion obtained from superposition were compared with the time-independent results, to investigate the time dependency of the solutions. The comparison and the satisfactory agreement between the results can be seen in Figure 10.

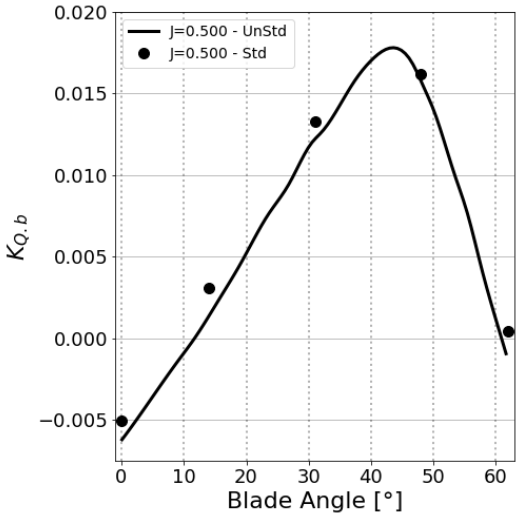

Fig. 10 The comparison of time-dependent and time-independent solutions (J =0.5)

The spindle torque coefficient dynamically calculated during the transient motion from full ahead pitch position (0°) to feathering position (62°) of a CPP at different advance coefficients is shown in Figure 8.c.

It is seen that the blade torque coefficients decreased with the increment in advance coefficients. This decreasing trend is associated with the reduction of the propeller loading due to the change in the advance coefficient. The spindle torque coefficient first increases with the start of the maneuver and then decreases after reaching a peak value (or a critical pitch angle). This curved behavior occurred in all advance coefficients. However, the peak value decreased with increasing advance coefficients. Furthermore, the blade angle at the peak value had larger angles with an increased advance coefficient. The pressure distribution on the propeller blade is investigated to explain how the peak values are created (Figure 11). The blade pressure surfaces and pressure distribution on the vacuum surfaces for different blade angles.

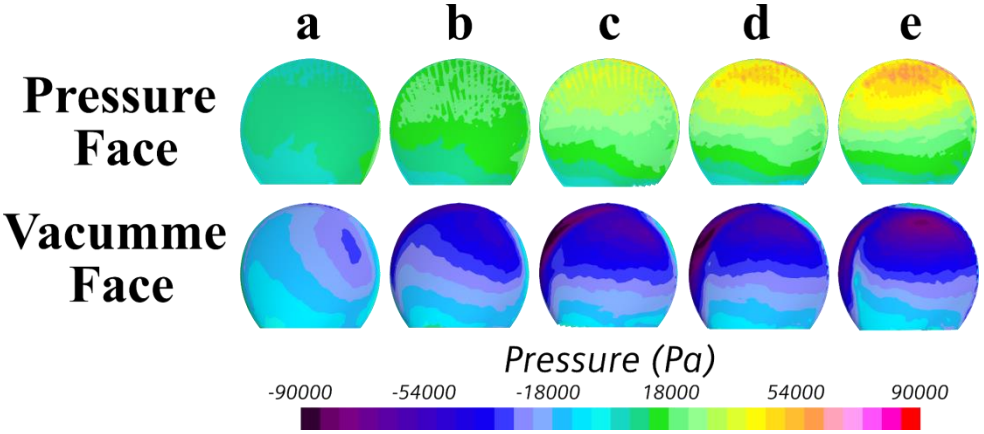

Fig. 11 a) 0°, b) 14°, c) 31°, d) 48°, e) 62° blade angle blade pressure and vacuum surface pressure distributions (J = 0.5)

The pressure distribution on the pressure and vacuum surfaces are balanced for the full ahead pitch position. However, the pressure values start to decrease on the vacuum surface near the leading edge especially in Figure 11.c and Figure 11.d with the increasing angle.

Figure 11.e shows that the low-pressure region on the vacuum surface at the feathering position spread to the back of the blade. To understand that the torque value was affected by pressure distribution displacement, Figure 12 shows the equal surface (iso-surface) of vacuum surfaces at a certain pressure distributions.

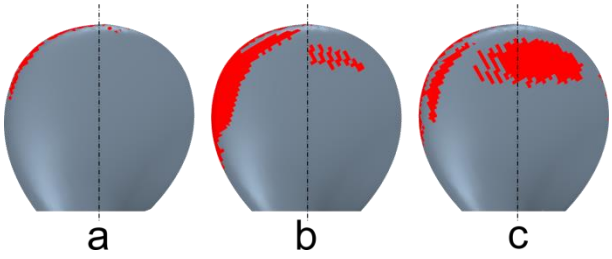

Fig. 12 a) 14°, b) 48°, c) 62° angles at vacuum surface for -60000 Pa value equal surface regions (J = 0.5)

Figure 12.a shows that a low-pressure region starts to form near the leading edge on the vacuum surface, the edge of the vacuum region expands to a larger region (Figure 12.b) and the vacuum region shifts from the edge to the back of the blade (Figure 12.c). The torque value on the blade is obtained by multiplying pressure difference regions and the distance of the obtained force to the rotation center. Thus, it can be seen that the low-pressure region was close to the edge until the peak angle value and high torque values occurred. When stalling occurred from this point to a higher angle value, the vacuum region shifted to the back of the blade and was distributed on the rotation center. This led to decreased torque value compared to the rotation axis of the blade.

The change of the propeller characteristics during the entire maneuver is given in Figure 13.

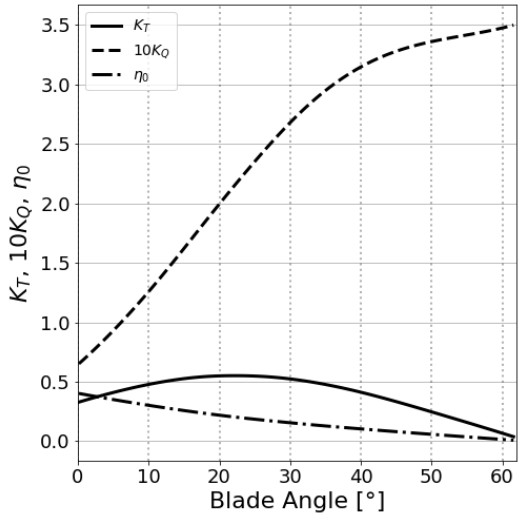

Fig. 13 Characteristic values of the propeller during the maneuver (J=0.5)

The propeller torque coefficient increased during the entire maneuver, this increase was rapid until the peak blade torque value pitch angle and the increase continued after reaching this angle despite the decreased rotation speed. Therefore, the propeller efficiency decreases during the entire maneuver and converges to zero.

5. Conclusion

This study presents the numerical investigation of the spindle torque variations on a CPP during the feathering maneuver. The feathering maneuver is a rare but challenging move in CPP operation and it is not well investigated yet. In order to generate a realistic numerical model, the time-dependent whole motion from full ahead position to feathering position was calculated dynamically using an overset/sliding mesh hybrid technique. DTMB 4119

propeller model, which is originally designed for the FPP use, was included in computations to see the availability of the FPP-CPP conversion. Results reveal that torque values are slightly lower in CPP use for the same propeller model, due to the geometrical modifications needed in the hub connection region. A novel non-dimensionalization equation to calculate the spindle torque values of a CPP was proposed. It is seen that the new equation's performance is better in the manner of representing the physical behavior and the trends in spindle torque variations. For the increasing pitch angles, spindle torque values for the CPP increases to a critical pitch angle, then decreases dramatically. This critical pitch angle reaches to higher values with the increment of advance coefficient. The flow characteristics in the hydraulic unit that controls the controllable-pitch propellers are directly related to the hydrodynamic performance. Therefore, it is recommended to consider the behavior of the hydraulic drive unit based on the data obtained in this study and the changes in blade angles in future studies. New hub designs are aimed to be examined to rotate the blades around the spindle axis. The damping behavior of flow-induced vibrations caused by the blades in fixed-pitch propellers in controllable-pitch propellers is also of interest. Additionally, examining the cavitation behavior on the blade and the acoustic output during superposition motion would also be valuable.

REFERENCES

[1] Wang, Y., Cao, L., Zhao, G., Liang, N., Wu, D., 2022. Experimental investigation of the effect of propeller characteristic parameters on propeller singing. *Ocean Engineering*, 256, 111538. https://doi.org/10.1016/j.oceaneng.2022.111538

[2] Jang, Y., Eom, M., Paik, K., Kim, S., Song, G., 2020. A numerical study on the open water performance of a propeller with sinusoidal pitch motion. *Brodogradnja*, 71(1), 71-83. https://doi.org/10.21278/brod71105

[3] Dogrul, A., 2022. Numerical prediction of scale effects on the propulsion performance of Joubert BB2 submarine. *Brodogradnja*, 73(2), 17-42. https://doi.org/10.21278/brod73202

[4] Peric, M., 2022. Prediction of cavitation on ships. *Brodogradnja*, 73(3), 39-58. https://doi.org/10.21278/brod73303

[5] Martelli, M., Figari, M., 2017. Real-Time model-based design for CODLAG propulsion control strategies. *Ocean Engineering*, 141, 265-276. https://doi.org/10.1016/j.oceaneng.2017.06.029

[6] Turnbull, W., 1931. Controllable-Pitch Propeller. *The Journal of the Royal Aeronautical Society*, 35(243), 231-244. https://doi.org/10.1017/S0368393100115810

[7] Martelli, M., 2015. Marine propulsion simulation: methods and results. *Walter de Gruyter GmbH & Co KG*.

[8] Nguyen, C., Luong, N., Ngo, V., 2018. A study on effects of blade pitch on the hydrodynamic performances of a propeller by using cfd. *Journal of Shipping and Ocean Engineering*, 8, 36-42. https://doi.org/10.17265/2159-5879/2018.01.005

[9] Ozturk, D., Delen, C., Belhenniche, S., Kinaci, K., 2022. The effect of propeller pitch on ship propulsion. *Transactions On Maritime Science*, 01, 133-155. https://doi.org/10.7225/toms.v11.n01.w09

[10] Chu C., Chan Z. L., She Y. S., Yuan V. Z., 1979. The 3-Bladed JD-CPP Series, *Proceedings of the 4th Lips Propeller Symposium*, Drunen, The Netherlands.

[11] Sheng CP, Chu C and Chan ZL. The estimation of blade spindle torque of controllable pitch propellers, *Proceedings of the 4th Lips Propeller Symposium*, Drunen, The Netherlands.

[12] Funeno, I., Pouw, C., Bosman, R., 2013. Measurements and computations for blade spindle torque of controllable pitch propellers in open water. *3rd International Symposium on Marine Propulsors*, Launceston, Tasmania, Australia.

[13] Rhee, S., Joshi, S., 2009. Cfd validation for a marine propeller using an unstructured mesh based rans method, *4th ASME-JSME Joint Fluids Engineering Summer Conference*, Honolulu, Hawaii, USA.

[14] Kolakoti, A., Bhanuprakash, T., Das, H., 2013. Cfd analysis of controllable pitch propeller used in marine vehicle. *Global Journal of Engineering Design and Technology*, 2(5), 25-33.

[15] Xiong, Y., Wang, Z., Qi, W., 2013. Numerical study on the influence of boss cap fins on efficiency of controllable-pitch propeller. *Journal of Marine Science and Application*, 12, 13-20. https://doi.org/10.1007/s11804-013-1166-9

[16] Bhattacharyya, A., Krasilnikov, V., Steen, S., 2016. Scale effects on open water characteristics of a controllable pitch propeller working within different duct designs. *Ocean Engineering*, 112, 226-242. https://doi.org/10.1016/j.oceaneng.2015.12.024

[17] Usta, O., Korkut, E., 2018. A study for cavitating flow analysis using DES model. *Ocean Engineering*, 160, 397-411. https://doi.org/10.1016/j.oceaneng.2018.04.064

[18] Zhou, X., Pan, H., Tian, X., Zhu, Z., 2019. Comparative analysis of hydrodynamic performance of propeller under different turbulence models. *Journal of Physics: Conference Series*, 300, 012-013.

[19] Arifin M., D., Faturachman, D., Octaviani, F., Sulaeman, K, A., 2020. Analysis of the effect of changes in pitch ratio and number of blades on cavitation on cpp. *International Journal of Marine Engineering Innovation and Research*, 5(4), 255-264. https://doi.org/10.12962/j25481479.v5i4.8285

[20] Pourmostafa, M., Ghadimi, P., 2020. Applying boundary element method to simulate a high-skew controllable pitch propeller with different hub diameters for preliminary design purposes. *Cogent Engineering*, 7(1), 1805857. https://doi.org/10.1080/23311916.2020.1805857

[21] Altosole, M., Martelli, M., 2017. Propulsion control strategies for ship emergency maneuvers. *Ocean Engineering*, 137, 99-109. https://doi.org/10.1016/j.oceaneng.2017.03.053

[22] Godjevac, M., Beek, T., Grimmelius, H., Tinga, T., Stapersma, D., 2009. Prediction of fretting motion in a controllable pitch propeller during service. *Proceedings of the Institution Of Mechanical Engineers Part M: Journal Of Engineering For The Maritime Environment*, 223, 541-560. https://doi.org/10.1243/14750902JEME128

[23] Martelli, M., Figari, M., Altosole, M., Vignolo, S., 2013. Controllable pitch propeller actuating mechanism, modelling and simulation. *Proceedings of the Institution Of Mechanical Engineers Part M: Journal Of Engineering For The Maritime Environment*, 228(1), 29-43. https://doi.org/10.1177/1475090212468254

[24] Jessup, S., Donnelly, M., McClintock, I., Carpenter, S., 2009. Measurements of controllable pitch propeller blade loads under cavitating conditions. *1st International Symposium on Marine Propulsors*, Trondheim, Norway. https://doi.org/10.5957/PSS-2009-06

[25] Tarbiat, S., Ghassemi, H., Fadavie, M., 2014. Numerical prediction of hydromechanical behavior of controllable pitch propeller. *International Journal of Rotating Machinery*, 2014, 180725. https://doi.org/10.1155/2014/180725

[26] Altosole M, Martelli M and Vignolo S.,2011 A mathematical model of the propeller pitch change mechanism for themarine propulsion control design. *Proceedings of the14th symposium on sustainable maritime transportationand exploitation of sea resources, IMAM 2011*, Genoa, Italy. https://doi.org/10.1201/b11810-98

[27] Liu, A., Dang, J., Xie, Q., Hu, J., 2015. The effect of sheet cavitation on the blade spindle torque of a controllable pitch propeller. *4th International Symposium on Marine Propulsors*, Austin, Texas, USA.

[28] Pourmostafa, M., Ghadimi, P., 2021. Unsteady simulation of marine controllable pitch propeller using boundary element method. *Journal of the Brazilian Society of Mechanical Sciences and Engineering*, 43, 47. https://doi.org/10.1007/s40430-020-02755-y

[29] Siemens, S., Star CCM+ Version 2020.3. User guide, n.d.

[30] Sezen, S., Bal, S., 2020. Computational and empirical investigation of propeller tip vortex cavitation noise. *China Ocean Engineering*, 34(2), 232-244. https://doi.org/10.1007/s13344-020-0022-8

[31] Jessup, S., 1989. An experimental investigation of viscous aspects of propeller blade flow, Ph.D. Thesis, The Catholic University of America, Washington.

[32] Sezen, S., Kinaci, O. K., 2019. Incompressible flow assumption in hydroacoustic predictions of marine propellers. *Ocean Engineering*, 186, 106138. https://doi.org/10.1016/j.oceaneng.2019.106138

Submitted: 08.01.2023.
Accepted: 05.04.2023.

Ahmet Yurtseven
Kaan Aktay
Department of Naval Architecture and Marine Engineering, Yildiz Technical University, 34349, Istanbul, Turkiye
ahmety@yildiz.edu.tr (ORCID: 0000-0003-2561-1783)